Experimental Mechanics (2024) 64:181–195
https://doi.org/10.1007/s11340-023-01018-w

RESEARCH PAPER

Residual Stresses in Alloy IN718 Produced Through Modulated Laser Powder Bed Fusion

K. Georgilas[1,2,3] · H. Guo[4] · B. Ahmad[4] · R. H. U. Khan[3] · M. E. Fitzpatrick[4] · M. E. Kartal[1]

Received: 29 May 2023 / Accepted: 6 November 2023 / Published online: 6 December 2023
© The Author(s) 2023

Abstract

Background Laser powder bed fusion (L-PBF) additive manufacturing (AM) is used for building metallic parts layer-by-layer and often generates non-uniform thermal gradients between layers during fabrication, resulting in the development of residual stresses when parts are cooled down.

Objective The impact of modulated laser used during the L-PBF process on residual stresses in Inconel 718 (IN718) material was investigated. The impact of build directions on residual stress is also determined.

Methods The contour method is employed to measure the full-field residual stress component on the cross-section of samples. A complementary residual stress measurement method, incremental hole drilling, was employed for obtaining in-plane residual stress components.

Results The results show that the residual stress distribution is sensitive to the build direction, with a higher magnitude of residual stress in the direction of build than that in the transverse direction. Multiple measurements with the same manufacturing parameters show good repeatability.

Conclusion Residual stresses in the as-built parts are significant and hence a further consideration regarding relieving residual stresses is required when post-thermal treatments are developed.

Keywords Residual stresses · The contour method · Alloy IN718 · Laser methods · Powder methods

Introduction

During laser powder bed fusion (L-PBF) processing, built parts are subjected to a complex thermal history of heating, melting, and subsequent cooling. As being based on a "layer by layer" manufacturing strategy, the L-PBF technique causes non-uniform temperature gradients generated between layers during fabrication, and hence shrinkage during solidification is anticipated at different levels in each layer, resulting in the development of residual stresses [1–4].

Residual stress is a stress state that remains within a body upon removal of external loading. Residual stresses can directly add to an applied external load and may cause failure even if the external load on its own, for instance, is not high enough to produce failure. In particular, tensile residual stresses are detrimental for many components that are subjected to cyclic loading, as tensile residual stress increases both the mean and the peak stresses. Therefore, understanding and quantifying residual stress that develops during L-PBF processes is vital to use components in safety-critical applications.

There are a number of methods to experimentally determine residual stresses in metallic materials. These methods can be broadly classified into two groups: destructive and non-destructive. Destructive techniques use the principle of releasing strain due to new surface creation by cutting or drilling, and deformation caused by residual stress relaxation is experimentally measured. Using deformation data measured, components of the residual stress can then be numerically and/or analytically calculated [5]. Non-destructive measurement techniques, on the other hand, involve probing

✉ M. E. Kartal
mehmet.kartal@abdn.ac.uk

1 University of Aberdeen, School of Engineering, Aberdeen AB24 3UE, UK

2 National Structural Integrity Research Centre, Cambridge CB21 6AL, UK

3 TWI Ltd., Cambridge CB21 6AL, UK

4 Coventry University, Centre for Materials and Manufacturing Engineering, Coventry CV1 2JH, UK

changes in crystal lattice parameters by means of beams of X-ray, synchrotron, or neutron, and by means of Bragg's Law lattice parameters are calculated. Laboratory-based X-ray diffraction provides in-plane residual stress components on and near to the free surface, whilst the neutron and synchrotron X-ray diffraction methods enable determination of residual stresses deep (up to several centimetres) within the material. However, neutron and synchrotron techniques are difficult to access with long lead times. More details regarding conventional residual stress measurement methods can be found elsewhere [5–7].

The contour method, invented by Prime [8] in 2001, is one of the most promising destructive residual stress analysis methods because it provides a 2D full-field residual stress map with a single cut, and is insensitive to the microstructure of a material. Experimental validations of the contour method have shown very good agreements with well-established residual stress measurement techniques such as X-ray diffraction [9, 10], neutron diffraction [11–14], synchrotron X-ray diffraction [15], slitting [16, 17], hole drilling [14, 18] and a combination of several methods [19] in the literature. The method has also been analytically validated for 2D geometries [20].

In the existing literature, there have been a few studies where residual stresses were experimentally determined in alloy IN718 manufactured by continuous L-PBF. Using the contour method, Ahmad et al. [2] measured residual stress in a cubic sample in the as-built condition. It was reported that the sample had compressive residual stress in the middle with a peak value of − 400 MPa and tensile stress of 800 MPa near to the free surface. Nadammal et al. [21] used neutron diffraction to investigate the influence of the hatch length processing parameter on residual stress generation. It was reported that the residual stress profile was affected by hatch length difference due to different thermal gradients. Longer hatch distance causes a larger residual stress gradient, particularly in the transverse direction. The normal stress component in the build direction is considerably compressive in a sample with shorter hatch length. Lu et al. [22] investigated the relationship between island scanning strategy and residual stress using Vickers micro-indentation. Although a scanning strategy with 2×2 mm^2 produced the lowest residual stress, it was found to be susceptible to crack formation. Therefore, 5×5 mm^2 was determined to be optimum. Goel et al. [23] studied the impact of scanning strategy on residual stress using neutron diffraction. Lower magnitude of stresses was found when a chessboard strategy was used instead of a bi-directional raster strategy.

In all the above-mentioned studies of residual stress [2, 21–23], the continuous L-PBF method was used to manufacture parts where the impact of a single processing parameter on residual stress was generally investigated. To the authors' best knowledge, residual stresses in alloy IN718 manufactured by modulated L-PBF have not been reported in the literature. It is known that parts produced by modulated L-PBF have similar phase composition (i.e., propagation of Laves phase) to ones produced by continuous L-PBF, but very different crystal microstructure in the build direction [24], which may cause a different state of residual stress. Therefore, there is a gap in the-state-of-art knowledge.

The principal aim of this work is to investigate residual stress fields in alloy IN718 samples developed during the modulated L-PBF additive manufacturing method. For this purpose, the contour method was employed to determine residual stress in samples with two different build directions, in the as-built condition. Residual stresses obtained from the contour method were compared with incremental hole-drilling data that were previously measured on replicate samples.

Materials and Specimens

Argon-gas-atomised alloy IN718 powder procured from LPW technology (Widnes, UK), with a size range between 15 µm and 45 µm, was used to manufacture all the test specimens in this study. Chemical composition, powder size distribution, flowability, and density of alloy IN718 powder were reported in an earlier study [24]. A Renishaw AM250 machine, that is based on L-PBF in the modulated laser mode, was used for manufacturing all the specimens. The optimised processing parameters that were identified elsewhere [24, 25] were used to produce specimens with the highest densification (~99.8%). The key L-PBF processing parameters in manufacture of the samples were: 200 W laser power; 110 µs exposure time; 140 µm hatch spacing; 60 µm powder layer thickness; and 60 µm point distance. The meander scanning strategy was used for building parts. For incremental hole drilling (IHD), six prismatic blocks of $30 \times 30 \times 10$ mm^3 were manufactured with and without support structures in the *XY* direction (Fig. 1(a)). Specimens to be measured using in the contour method were manufactured with dimensions of $50 \times 20 \times 10$ mm^3 and built in the *Z* (Fig. 1(b)) and XY (Fig. 1(c)) directions. Here, *Z* refers to the longest axis of a specimen that is perpendicular to the plane of the substrate (i.e., vertical specimen) and *XY* refers to the longest axis of a specimen built along the plane of the substrate (i.e., horizontal specimen). All the specimens used for the contour method were built with support structures on the substrate. Figure 1 also shows the global coordinate system and the build direction of specimens. Table 1 summarises sample orientations, build conditions and stress measurement methods used.

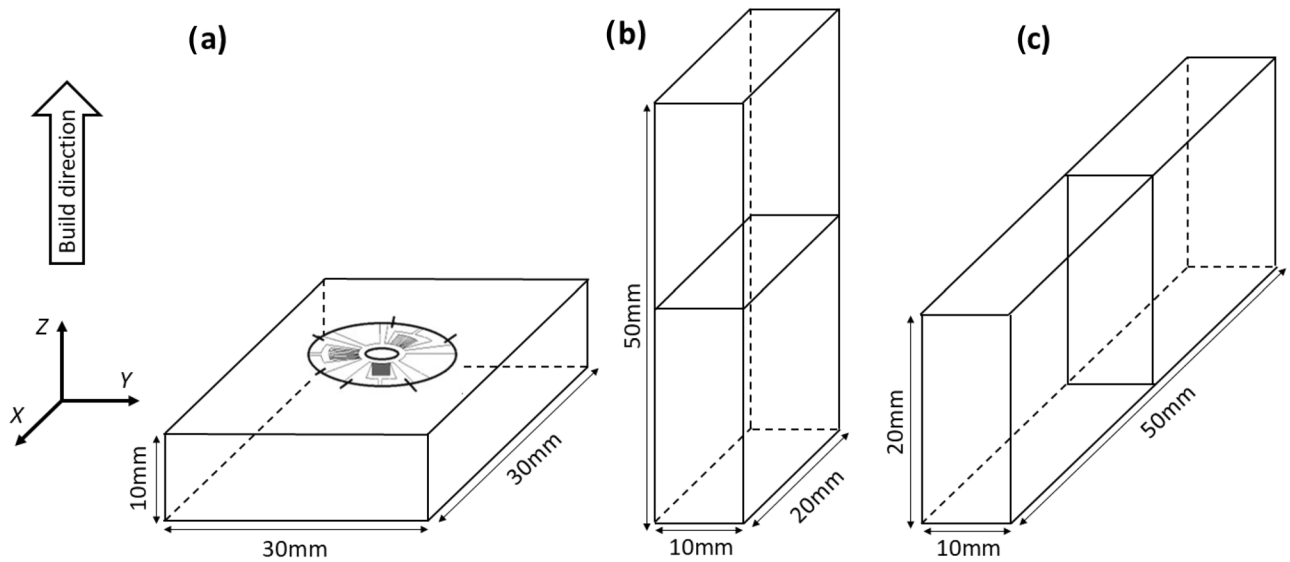

Fig. 1 Specimens used for residual stress measurements. (**a**) the incremental hole drilling specimen with location of the strain gauge, (**b**) the contour method specimen built in the *Z* direction, (**c**) the contour method specimen built in the *XY* direction. The rectangle at the midplane in Fig. 1(b) and (c) is a plane of the contour cut

Residual Stress Analysis Methods

In this work, the contour method for residual stress analysis was used. Given that a 2D residual stress map with a single cut can be obtained with widely available equipment, without having to access national laboratories, and that a number of the L-PBF processed components were to be measured, the contour method appeared to be the ideal technique to employ. However, the main drawback with the contour method is that it provides only a single residual stress component normal to the cut surface. Hence complementary semi-destructive hole-drilling results reported in our previous work [24] were used to compare multi-axial residual stress components in alloy IN718.

Hole Drilling Method

Incremental hole drilling (IHD) can be used to determine in-plane residual stress components as a function of depth along a drilled hole. This can be achieved by placing strain gauges on the free surface of a specimen and drilling a hole through the centre. In this way, in-plane strains caused by stress relaxation are experimentally measured as a function of depth from the free surface. The measured strain components are then used to determine the in-plane residual stress components on the plane perpendicular to the axis of the hole. Therefore, this method provides a 1D profile of the 2D residual stress components normal to the drilling direction. The measurement method and calculation of residual stresses followed a method based on ASTM standard E837-13a [26] and was previously reported [24]. A 1/8th inch nominal type 'A' strain gauge rosette was glued on the top surface of each specimen. The rosette includes three strain gauges, each of which was connected to a PC via an amplifier. Considering the global coordinate system and the schematic of a specimen used for hole drilling in Fig. 1, positioning the strain gauge rosette on the top surface of each specimen permits the measurement of σ_{xx}, σ_{yy} normal and τ_{xy} shear stresses.

Even though porosity in the samples was low, standard drill bits might not be a good option to use as they can be deflected when they are in contact with a pore, resulting in failure of drill bits. Therefore, an AJ-1 air abrasion machine made by Texas Airsonics (Texas, USA) was employed to drill holes by means of pure silica sand. Since controlling

Table 1 Specimen numbering, orientation and test method for the current work

Specimen number	Orientation	Condition	Test method
Specimen 1–3	*XY* (horizontal)	Supports	Incremental hole drilling
Specimen 4–6	*XY* (horizontal)	No Supports	Incremental hole drilling
Specimen 7–9	*Z* (vertical)	Supports	Contour method
Specimen 10–12	*XY* (horizontal)	Supports	Contour method

the depth of a hole with air abrasion was not feasible, a two-minute interruption between the drilling steps was introduced to follow the ASTM standard until the hole reached a total depth of 1 mm. Several trials were attempted on spare material to select the air abrasion parameters (i.e., pressure, offset distance) to achieve the required hole diameter and step depth. The final holes were performed at an offset distance of 7.5 mm and a pressure of 5.5 bar, which were found to achieve a nominal step depth of 0.2 mm in accordance with ASTM E837-13a for the selected type of strain gauge. Dimensions of the hole after each step were probed with a calibrated focusing scope to inspect the depth and circularity of the hole, as well as to determine the shape of the bottom. After each drilling step it was found necessary to wait until the specimen cooled down to reach ambient temperature before measuring strains. Eval 7 software by SINT technology (Florence, IT) was used for processing experimental data. The residual stresses were assumed to be non-uniform, and the integral method was employed to calculate residual stresses as described in the ASTM standard.

Contour Method

The contour method is a destructive method that allows measurements of residual stress at both small and large cross-sectional areas with a single cut [8, 27, 28]. The method has significant advantages in terms of implementation and interpretation as discussed elsewhere [29, 30]. The principle of the contour method is simple. First of all, a sample in which residual stress is to be determined is cut into two halves, resulting in stress relaxation on the cut surfaces. Then the displacement components normal to both the cut surfaces are experimentally measured. Since experimental measurements almost always include noise, which is not a result of stress relaxation, the averaged displacements of both the cut surfaces are fit by a smooth analytical function typically using Fourier series [8, 20] or polynomials [2, 27, 30]. The implementation of the contour method then follow to model the half part of a sample where all the surfaces are traction-free except for the cut surface, which is subjected to prescribed boundary conditions using the averaged and fit data in the normal direction, and unconstrained in the shear directions (shear stresses are assumed to be zero). Here, the residual stress component normal to the cut surface can be directly calculated from displacement component by means of an elastic solution with minimal computational cost and time. However, the residual stress component obtained is valid only on the plane of a cut.

For this work six specimens were used for the contour method. EDM cutting and CMM measurement were performed at Coventry University. Cuts were performed using a Fanuc Robocut α-C600i (Fanuc, Yamanasi, Japan) wire electro-discharge machine using a 0.25-mm-diameter brass wire. The samples were symmetrically clamped, and water injection nozzles were used. To produce high quality cuts that minimize cutting induced stresses, optimal parameters as identified in the previous work of Ahmad et al. [2] were used. Figure 1(b) and (c) shows schematic planes of the cut in the specimen where displacement distributions were measured in the direction normal to the cut surface. An example of cut surfaces (top surfaces of the cut pair) is shown in Fig. 2 for an actual specimen. In the red box, the support structures of the specimen can be seen. Sectioned profiles were measured using a Zeiss Contura g2

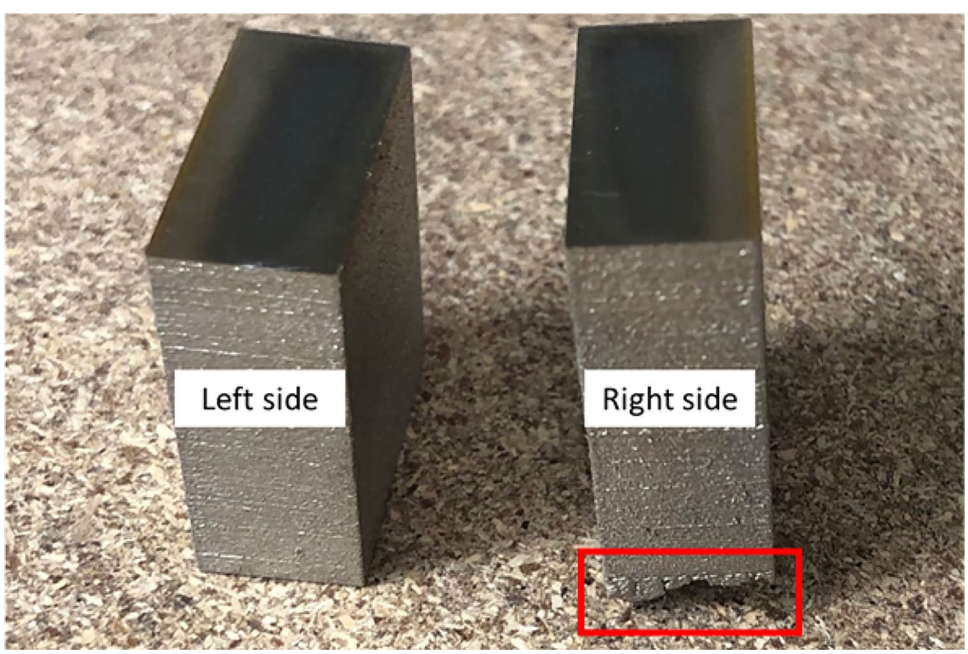

Fig. 2 A picture of the contour method specimen after the EDM cut. The support structure of the material is seen in the red box

CMM using a 3-mm-diameter touch probe. Each cut plane (e.g., left-side and right-side in Fig. 2) was measured using a 0.2 mm spaced grid. Outlines of each cut surface were also measured to aid the finite element modelling setups.

Data analysis involves aligning the data for both the cut surfaces of a specimen, bringing them to the same coordinate system, and averaging them. Since the measured displacement component normal to the cut surface is a result of both the normal and shear stress relaxation after cutting, it is necessary to average displacement data to cancel out the contribution of shear stress relaxation in the normal displacement component, so that the correct normal residual stress component can then be calculated. Averaging of data is also important for removing possible noise or artefacts in data caused by the cutting process or due to uncertainty of the measurement [11, 31]. Averaged data are then cleaned to remove possible noise and artefacts. However, cleaned data still possess noise caused by measurements and noise is not due to stress relaxation. Hence, there is a need for the use of fitting the averaged and cleaned data to an analytical function, otherwise it produces an amplified effect during the calculation of residual stresses. The most-used tool for smoothing the data is spline fitting, as these functions are found in piecewise polynomial form and hence it is flexible to adjust spline parameters suitable to any arbitrary contour profile. In the current work, cubic spline fitting [32, 33] was used to join polynomials at a number of intervals (knotspace) to form a smooth spline. Data smoothing was performed using MATLAB (Mathworks, Massachusetts, USA).

A 3D finite element model for residual stress calculation was built for one half of each of the six samples. Modelling was performed using SIMULIA Abaqus FEA (Dassault Systems, Vélizy-Villacoublay, France). The models were meshed using linear hexahedral elements with reduced integration. It was assumed that each specimen was elastic with 201 GPa Young's modulus and 0.294 Poisson's ratio. Averaged and fit displacements were reversed in sign [8] and imposed as prescribed boundary conditions on the cut surface. An equilibration step was taken for each model and residual stresses were calculated on the cut surface.

Results

Incremental Hole Drilling

Table 2 below shows the diameter and maximum depth of the hole for each IHD sample. It was noted that the depth of each hole varied between 0.96 mm and 1.02 mm, due to the time-based aspect of the drilling method, leading to variations in the depth of the hole after each step. In terms of hole diameter only specimen 2 falls below the required value, by ASTM E837-13a, for non-uniform residual stress calculation, by 70 µm. Abrasion was found to lead to a circular hole with a square bottom with fillets. Occasionally, small porosity was seen via the focusing scope, on the side walls of holes.

Table 2 Maximum hole depth and hole diameter for incremental hole drilling specimens

Specimen number	Maximum depth (mm)	Hole diameter (mm)
1	0.98	3.96
2	1.02	3.79
3	0.96	3.88
4	0.98	3.87
5	1.00	3.89
6	1.02	3.86

Figure 3 shows residual stress variations as a function of position through the hole depth for the IHD specimens with support (a) and without support (b) structures. The in-plane residual stress components of the IHD specimens in Fig. 1(a) are σ_{xx}, σ_{yy} and τ_{xy} (see the coordinate system in Fig. 1).

In the samples with support structures, normal stress components are tensile between 70 to 460 MPa, and their values increase with hole depth. For the unsupported specimens, the normal stress components varying between – 7 MPa to 159 MPa do not show strong correlation with the hole depth. Shear stress in both the cases is mostly negative and does not vary with the hole depth. For the specimens with supports shear stress ranges from 33 MPa to –42 MPa, while for those without support varies from 11 MPa to – 56 MPa. Since the IHD tests were performed on three replicate samples for each sample condition (i.e., supported and unsupported), the standard deviation and errors were calculated by using residual stress values measured at each step of hole increment in each replicate sample. The uncertainty of measurements was found to be higher in specimens 4–6 (30% on average) versus specimen 1–3 (20% on average). The scatter between measurements is the highest at the first step of IHD for both types of specimens, before decreasing with increased the hole depth.

Contour Method Results

Figure 4 shows the measured and averaged displacement of two mating surfaces of contour specimen 8 (a) and corresponding spline fitting plots with knotspace 1 (b), knotspace 3 (c), knotspace 5 (d), knotspace 7 (e) and knotspace 9 (f). The maximum-to-minimum range of the contours is 0.01 mm to – 0.025 mm. It can be seen that with increased knotspace the final surface becomes more detailed. It is important to determine the knotspace used to obtain the optimum fit to data such that averaged displacement data are not overfitted or underfitted. Underfitting does not

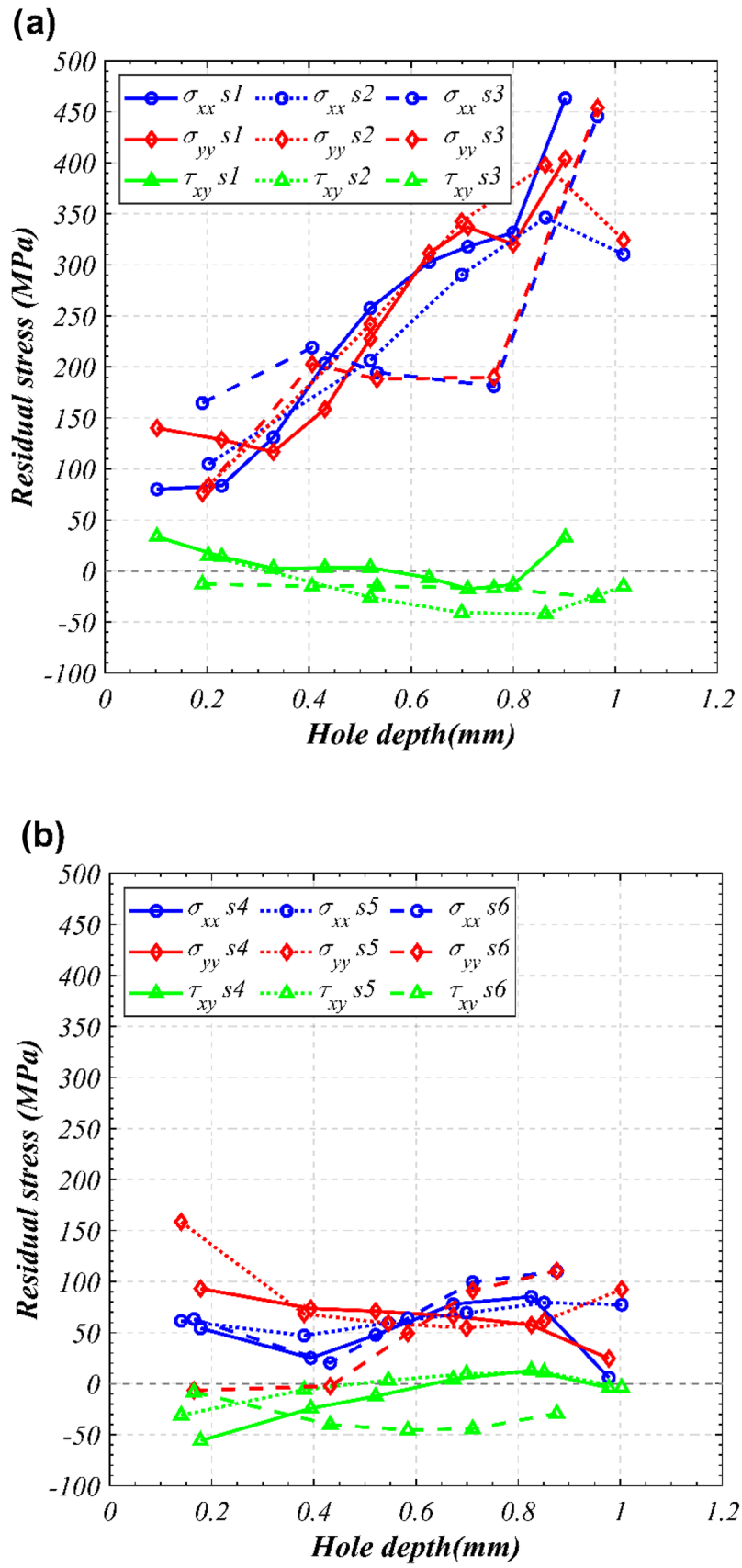

Fig. 3 Measured residual stress versus hole depth for specimens with supports (**a**) and without supports (**b**). *s* in the legends stands for 'specimen'. Sample details are provided in Table 1

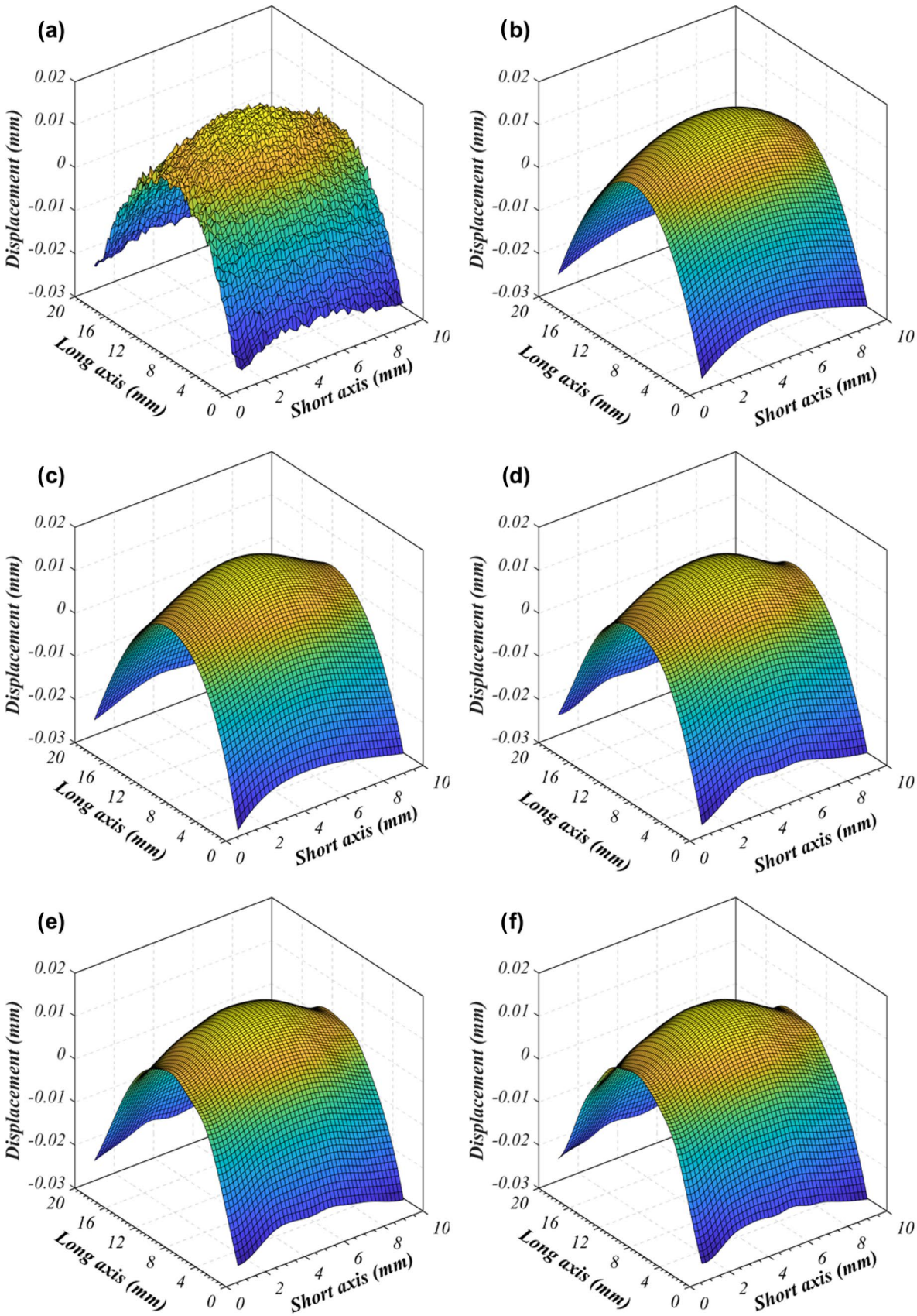

Fig. 4 Averaged data of specimen 8 (**a**) and its spline fitting for knotspace 1(**b**), knotspace 3 (**c**), knotspace 5 (**d**), knotspace 7 (**e**) and knotspace 9 (**f**)

provide enough resolution, resulting in missing peak values and detailed stress distribution; while overfitting causes intensification of the stress magnitudes due to smoothing experimental noise which is not caused by stress relaxation. For all the specimens the optimum knotspace was found to be 3, which corresponds to 3 piecewise spline functions connected to each other end-to end.

The optimum knotspace was decided by comparing agreement between measured and averaged displacements and their fit using 2D line plots. Here, it is important to note that selected spline knotspace represents the best compromise between smoothing the noise in the measured data and fitting the underlying surface profile. Figure 5 shows comparison between averaged displacement and its fit data with knotspace 3 in the vertical (a) and horizontal (b) directions of specimen 8. It can be seen that the spline function with knotspace 3 defines averaged data well without fitting short-range fluctuations in the averaged data.

Figure 6 shows a compilation of the residual stress fields for the vertical (7, 8, 9) and horizontal (10, 11, 12) contour specimens. Considering the global coordinate system in Fig. 1, the measured single residual stress component with the contour method is σ_{zz} for the vertical and σ_{xx} for horizontal specimens. All the results are shown with constant contour colouring ranging from − 450 to 750 MPa. The minimum value (− 450 MPa) is the greatest compressive stress demonstrated in the results while the maximum value (750 MPa) is the yield strength of the material [25].

The specimens built in the *Z* direction (7, 8, 9) show grey areas along the top and bottom which suggest the stress field is above the yield strength of the material, but below the UTS and thus plastic deformation might have taken place. This matter will be discussed in the following section. Specifically, a maximum of 950 MPa was found for specimen 7, 1097 MPa for specimen 8, and 996 MPa for specimen 9. In terms of the stress maps, they show consistent distribution with the centre of the specimens being under compression while the smaller sides of the outline show significant tensile stresses. The longer sides of the outline also generally show low tensile stress.

Horizontal build specimens (10, 11, 12) also show compressive stress in the centre, varying from –200 to –270 MPa. However, for the tensile stresses a different morphology is seen. For the edge close to the substrate (towards *Z'*) a slight tensile stress can be seen of around 200 MPa. For the edge away from the substrate (at *Z*) the tensile stress is higher at between 420 to 500 MPa. Hence, there is an imbalanced tensile stress between the two sides. Most of the long edges, however, still show a tensile stress of about 150 MPa. In order to compare the results of six contour specimens, stress values along the long axis (at $Y = 0$ mm) and the short axis (at X or $Z = 0$ mm) in Fig. 6 are extracted and plotted in Fig. 7(a) and (b), respectively. These curves qualitatively show variations of residual stress field through the geometry of the specimens.

It should be noted that when the optimum processing parameters for contour cutting are in place as stated in "Contour method" section, and displacement measurements, data manipulation and residual stress calculation are appropriately carried out (as was successfully demonstrated in the previous work of Kartal et al. [11, 31] where a good agreement between the neutron diffraction and the contour method was achieved), uncertainty associated with results of the contour method could be about 10%; although part size directly affects uncertainty where smaller parts produce smaller deformation caused by residual stress relaxation and hence uncertainty likely increases [34].

Since specimens 1, 2 and 3 for IHD and 10, 11 and 12 for the contour method were built in the XY (horizontal) direction with support structures; and the same stress component (σ_{xx}) with respect to the global coordinate system in Fig. 1 was measured in all these specimens, it is possible to compare the residual stress profile obtained from two residual stress measurement methods in Fig. 8. The contour method results reach their maximum tensile values of 450–480 MPa at 0.2–0.35 mm from the free surface and then progressively reduce with distance. The hole drilling results increase continuously with depth. As can be seen from this figure, each measurement method employed produces similar residual stress profiles between three replicate samples. The contour method results show higher residual stress values than the hole drilling ones.

Discussion

Incremental Hole Drilling

Hole drilling measurements exhibit normal residual stress components in a range of − 7 to 160 MPa for the samples without supports in Fig. 3(b). On the other hand, the measured normal residual stress components (σ_{xx} & σ_{yy}) for the specimens with supports in Fig. 3(a) are significantly higher. The highest normal tensile residual stresses measured was 460 MPa. Additionally, the supported specimens show increasing residual stress with increasing hole depth.

The specimens directly built on the substrate plate without support structures (i.e., specimens 4, 5 and 6) possess a lower magnitude of residual stress than those with support structures (i.e., specimens 1, 2 and 3). This difference can be attributed to different heat transmission in the build direction due to the surfaces with which specimens are bounded. The specimens without support structures (specimens 4, 5 and 6) have a larger heat exchange area with the substrate plate while those specimens with support structures (specimens 1, 2 and 3) have a heat exchange

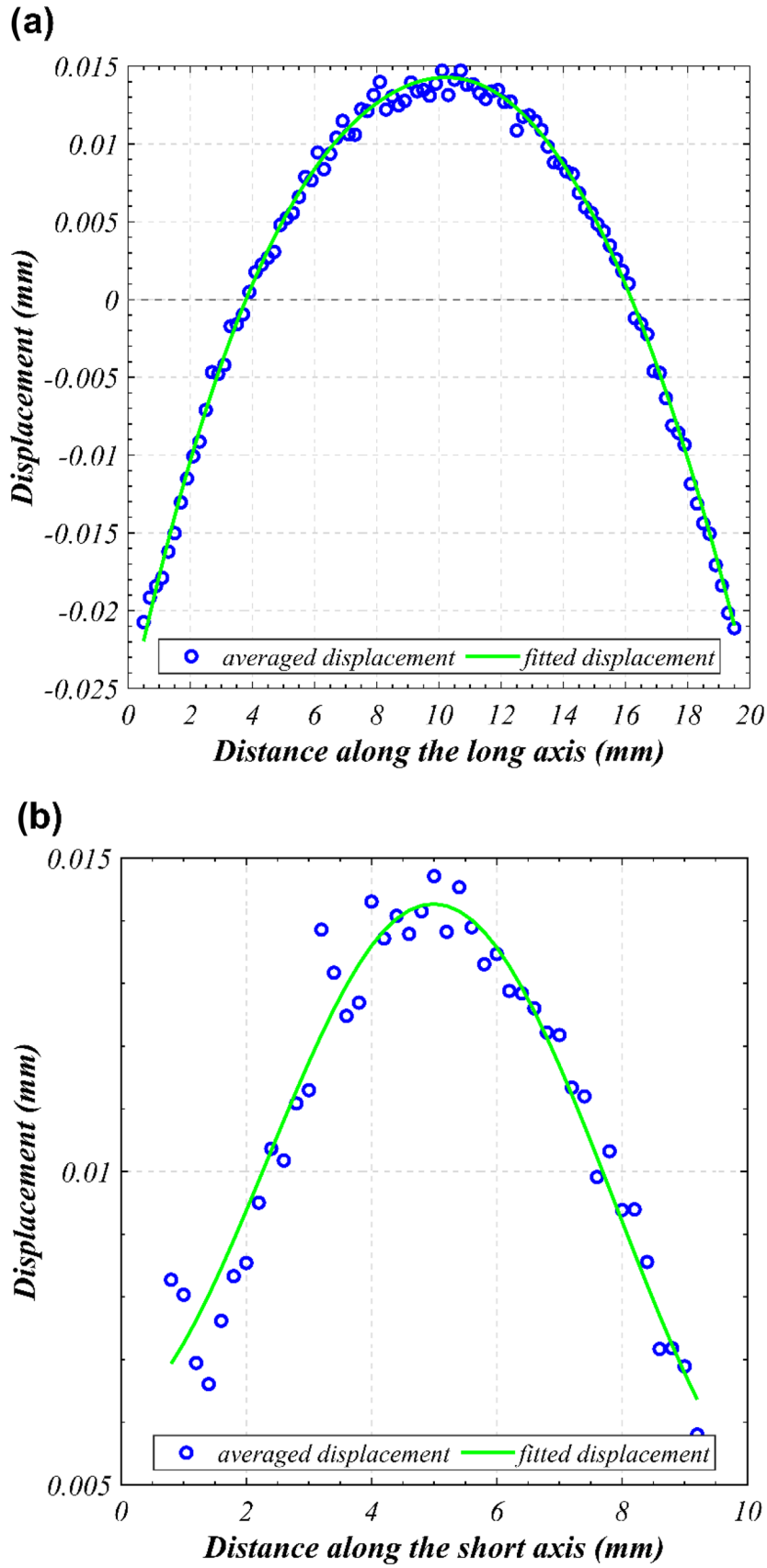

Fig. 5 Measured and averaged data of specimen 8 and its spline fitting with knotspace 3 along the vertical (**a**) and horizontal (**b**) directions on the cut surface

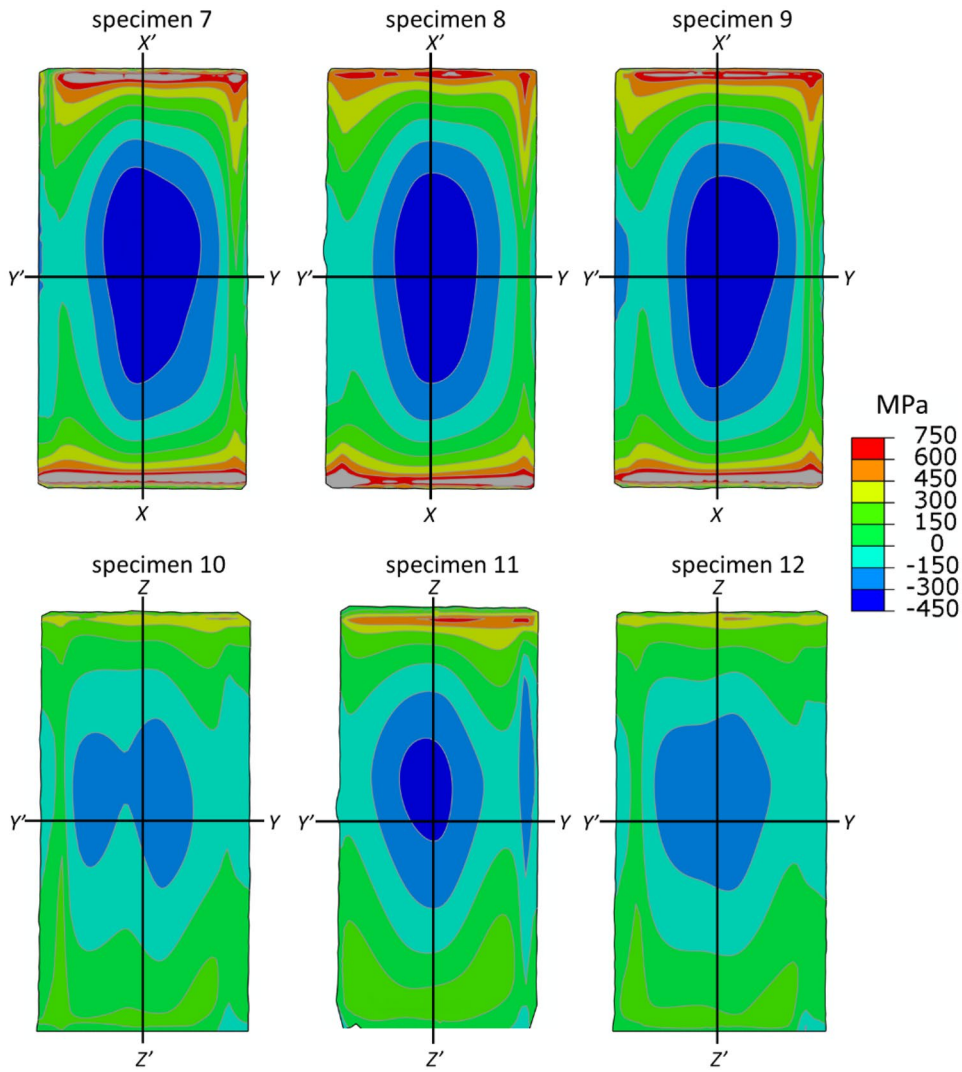

Fig. 6 Residual stress fields for the vertical (7, 8, 9) and horizontal (10, 11, 12) specimens calculated using the contour method. Sample details are provided in Table 1

surface which is limited to the support section. Therefore, temperature gradient in the specimens without support is lower, resulting in lower residual stress magnitudes. The increase in measured residual stresses in the specimens with support structures occur because the stress balances within the whole volume of the manufactured component, with localised areas showing variability in the stress field [35–37]. Similar behaviour with and without support structures was previously observed in AlSi10Mg [38].

In both the supported and unsupported specimens, the two residual stress components (σ_{xx} & σ_{yy}) were closely aligned to each other, following the same trends. The alignment of these two stress components has been observed in continuous L-PBF, attributed to the scanning strategy in the work of Robinson et al. [39] when the scanning was performed in a checkerboard pattern. Hence, in terms of residual stress, the pulsed L-PBF meander strategy leads to the same results as the continuous checkerboard.

At this point it should be noted that the measured stresses at the top of the specimen might be affected by the surface preparation carried out. Specifically, strain gauges can only be attached on smooth surfaces, which necessitates polishing. However, polishing the surface removes material and may modify residual stresses at the top surface of specimens, making measurements close to the edge unreliable. Other issues with performing hole drilling residual stress measurements on L-PBF material exist. First, the presence of porosity within the L-PBF specimens affects the residual stress. Since the porosity distribution is random for each sample even though the same processing parameters are used, a residual stress profile measured by hole drilling may be affected by porosity. Another issue, as presented by Karabulut and Kaynak [40], is the possible effect of work hardening the material during drilling. The final point is the impact of the use of air abrasive drilling (instead of high speed or conventional drilling) on the measured residual

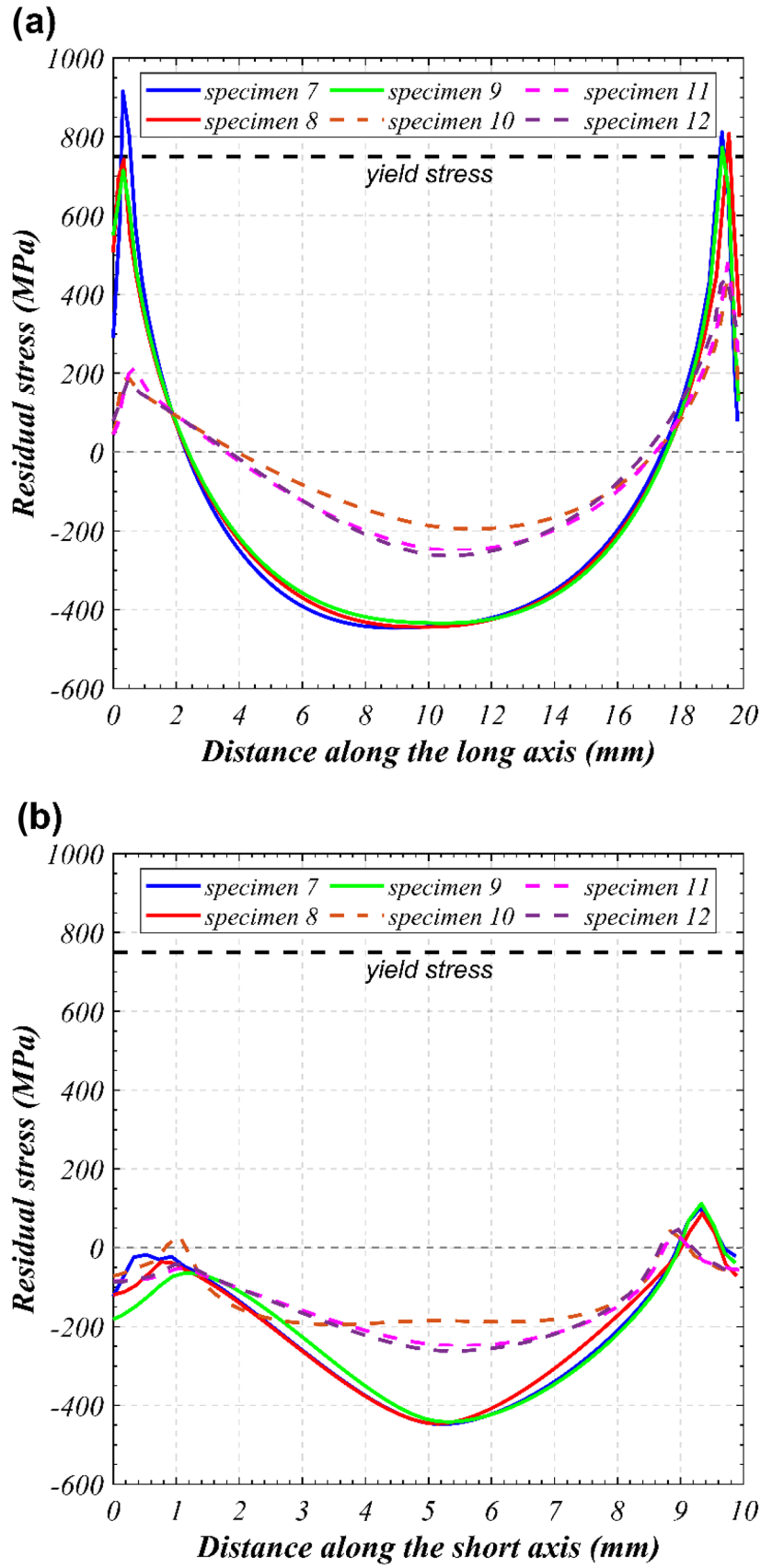

Fig. 7 Comparison of residual stress field for specimens shown in Fig. 6 along the (**a**) long axis and (**b**) short axis. For specimens 10–12 the substrate is close to the left of the figure where the measured residual stress is lower. The black dashed line denotes the yield strength of the material. Sample details are provided in Table 1

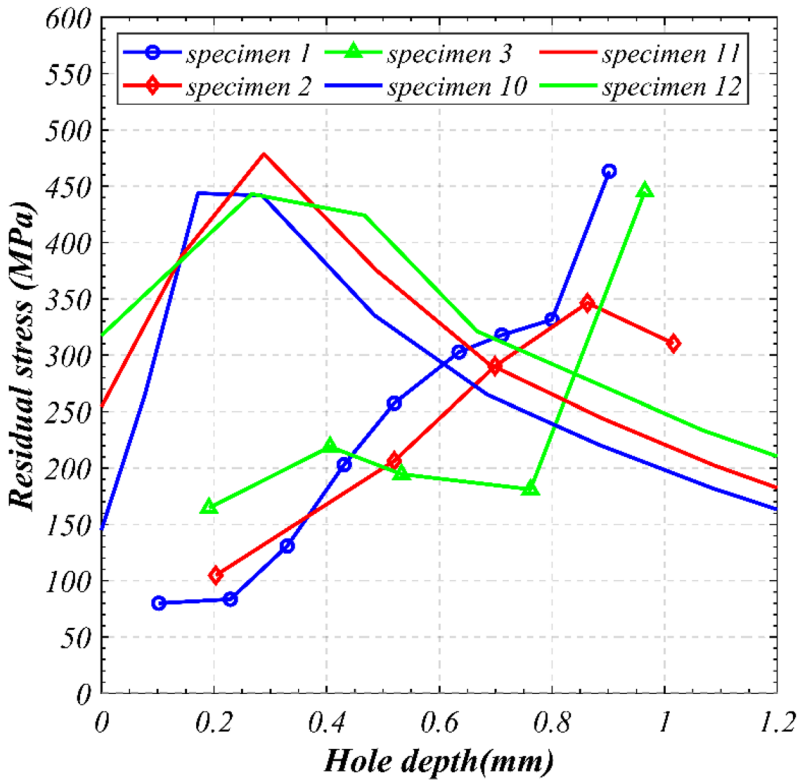

Fig. 8 Comparison of measured residual stress of the contour method versus hole drilling method. For specimens 1–3 (IHD) the actual hole depth is higher due to the surface polishing required for the application of the strain gauges. For specimens 10–12 (the contour method), stress field begins at the edge of the surface. Sample details are provided in Table 1

stress values. Previous studies with hole drilling measurements on conventionally manufactured specimens with low residual stress revealed that measurements with air abrasive drilling and high-speed drilling give a standard deviation of 14 MPa among the measurements [41, 42], suggesting reliable results with air abrasive drilling may be obtained.

Despite air abrasion being a viable method for implementing IHD for conventional materials, this is not completely the case in our study. The calculated uncertainty was found to be high for the unsupported specimens by reaching up to 66% for the first step with an average scatter of 30% for the whole data set. The supported specimens show lower uncertainty with the first step reaching 30% and an average scatter of 20%. Hence, it can be said that the preparation required to perform IHD experiments and the complex microstructure (particularly porosity) in the L-PBF specimens lead to high scatter in the measurements. Methodology to decrease the scatter would be to ensure that specimens have minimal internal defects and the surface to be drilled is as flat as possible, by adjusting the L-PBF parameters. Using conventional drilling and/or improving the application measurements of air abrasion drilling might also lead to improvements in reproducibility.

Contour Method

The stress maps obtained by employing the contour method as shown in Fig. 6 demonstrate a clear difference of residual stress distributions between the build orientation of the specimens. The difference in the stress magnitude between contour specimens built in the *XY* and *Z* directions may be attributed to differences in heat transfer during solidification due to the different build section and build height.

The vertical-build (*Z* direction) specimens reveal a symmetric stress field with high stress concentration at the narrower ends of the section. On the other hand, the horizontal-build (*XY* direction) specimens show obvious signs of the stabilising effect of the substrate plate. The stress field in the *XY* specimens does not show symmetry, with stress being higher at the top of the specimen and lower closer to the substrate plate. Thus, the support structures do not completely isolate the specimens from the substrate plate in terms of residual stress generation. Hence, that is the reason for why the residual stress field for the *XY* specimens is not symmetrical through the measured plane. It is evident that the support structures decrease the impact of the substrate plate on the residual stress field, but do not completely remove it. This leads to a difference of ~ 150 MPa in the measured stress between the top and bottom of the *XY* specimens. This is an important consideration to keep in mind when designing parts to be manufactured by this method.

Very little published literature exists of the contour method applied to alloy IN718 L-PBF material. Specifically, Ahmad et al. [2] performed the contour method on an alloy IN718 cube produced through continuous L-PBF. Like the current work, scanning was rotated 67° between

layers and followed a meander scanning pattern. The σ_{zz} stress field of the vertical specimen was calculated, and the results reported were in line with those produced in the current work, with stress being highest in two areas running parallel to the top and bottom perimeter of the projection, and compressive in the middle of the specimen.

It has been shown in the literature that the residual stress field largely depends on the scanning pattern of a heat source [43]. However, as shown in [24] the intermittent heating of the modulated power laser causes a different crystal microstructure in the material compared to the continuous L-PBF process. Hence, a question arises regarding the similarity of the measured residual stress fields between the two methods (continuous & modulated power) despite the microstructural differences. However, the question can be answered if the distance at which the heating-cooling cycle affects the developing residual stress field is considered. Specifically, as Mercelis and Knuth [1] have demonstrated, the interaction between the current layer (n) and the previous layer ($n-1$) will lead to the production of tensile stress at the top of the specimen. This tensile stress will be balanced by the accumulation of compressive stress inside the specimen at a distance from the current layer (n) and even by interaction with the substrate plate, as demonstrated by the current work's horizontal-build specimens. On the other hand, crystal microstructure is also affected by the heating-cooling cycles, but this effect is limited to the last few (~5) layers of the consolidated material. Hence, the difference between continuous and modulated power heat sources arises due to the different scanning pattern (continuous scanning versus successive point scanning), causing differences in crystal microstructure, and not longer-scale phenomena such as residual stress build-up.

A final point to be discussed regarding the contour method results in this work is the yield stress and plastic deformation. Residual stresses are elastic stresses that balance within a component. Hence, after data analysis and modelling, the produced stress field should be in the elastic region, below the yield strength of the material. The current work has found regions where the residual stress is above yield stress, suggesting plastic deformation might have taken place. However, although the single residual stress component has values in some small regions that are greater than the yield stress of alloy IN718, the hole drilling and contour method results in this work show that residual stresses in the samples are considerably multi-axial at the same locations. It follows that maximum residual stress values, in view of the von-Mises theorem, may not be beyond the yield stress as was observed elsewhere for components manufactured by various welding techniques [27, 44]. In any case, residual stress above the yield stress is found only within the tiny bands at both the bottom and top edges, and hence only localised plastic strain around the bands may be anticipated in the specimens after cutting. It follows that there is no significant impact of the plastic deformation on residual stress redistribution in the remainder of the cut plane where residual stress is well-below the yield stress.

It should be also noted that the tiny grey bands where local plastic deformation might have occurred were the locations at which an EDM wire entered and exited the specimens. Stress concentration caused by the wire is unavoidable at those regions and produces wire entry/exit artefacts [30]. When high-magnitude residual stresses (relative to the yield strength) are present in the zone, plastic deformation may occur followed by strain hardening. Unlike specimens 7–9 where tiny grey bands exist, specimens 10–12 do not possess such regions, as the existing residual stress magnitudes in those specimens are low enough to remain in the elastic zone during cutting. However, local stress concentrations at both the bottom and top regions can be still observed, and this justifies the conclusion that EDM wire caused local plastic deformation in those edges due to stress concentrations.

Method Comparison

Figure 7 compared the residual stress profile obtained from the hole drilling and contour methods. The figure shows that there is difference in the measured stress field between the two methods. This difference can be explained as the dimensions of the specimens being different for the two measurement techniques (Fig. 1(a), (c)). It is therefore expected that the heat transfer and cooling characteristics are different during the fabrication of the different specimen types. In consequence, it may be expected that the residual stresses are different. In addition, the specimens used for each method require significantly different preparation. The contour method requires little-to-no specimen preparation, while hole drilling requires the removal of material by grinding/polishing to attach the strain gauge. Thus, the stress field measured by hole drilling will have been affected by the preparation, while the contour method results are less affected by the procedure [8].

Conclusions

- The contour method can be successfully employed to characterise the residual stress in alloy IN718 produced by the modulated L-PBF material.
- Higher residual stresses are seen for the vertical-build samples compared to horizontal-build. Stresses are high and tensile at the surface, and compressive in the centre of the samples.

- Support structures lead to higher measured residual stress close to the top of the material compared to when no support structures are present.
- Vertical-build specimens show tensile residual stress at the edge of the material, whose magnitudes exceed the yield stress of the material, which is possibly an artefact of the cutting process.
- Horizontal-build specimens show residual stress fields comparable to those found by hole drilling.
- Further development of the hole drilling method for L-PBF material could be a useful tool for semi-destructively characterisation of produced parts.

Funding The work was financially supported by the Lloyd's Register Foundation, United Kingdom, a charitable foundation helping to protect life and property by supporting engineering-related education, public engagement and the application of research. The authors would also like to thank the National Structural Integrity Research Centre (NSIRC) United Kingdom, a postgraduate engineering facility for industry-led research into structural integrity established and managed by TWI through a network of both national and international Universities.

Data Availability The raw data required to reproduce these findings cannot be shared at this time as the data also forms part of an ongoing study. The processed data required to reproduce these findings cannot be shared at this time as the data also forms part of an ongoing study.

Declarations

Ethical Statment This manuscript does not contain any studies with human participants or animals.

Conflict of Interests The authors declare that they have no conflict of interest with other people or organizations.

Open Access This article is licensed under a Creative Commons Attribution 4.0 International License, which permits use, sharing, adaptation, distribution and reproduction in any medium or format, as long as you give appropriate credit to the original author(s) and the source, provide a link to the Creative Commons licence, and indicate if changes were made. The images or other third party material in this article are included in the article's Creative Commons licence, unless indicated otherwise in a credit line to the material. If material is not included in the article's Creative Commons licence and your intended use is not permitted by statutory regulation or exceeds the permitted use, you will need to obtain permission directly from the copyright holder. To view a copy of this licence, visit http://creativecommons.org/licenses/by/4.0/.

References

1. Mercelis P, Kruth J (2006) Residual stresses in selective laser sintering and selective laser melting. Rapid Prototyp J 12(5):254–265
2. Ahmad B, van der Veen SO, Fitzpatrick ME, Guo H (2018) Residual stress evaluation in selective-laser-melting additively manufactured titanium (Ti-6Al-4V) and inconel 718 using the contour method and numerical simulation. Addit Manuf 22:571–582
3. Kalentics N, Boillat E, Peyre P, Gorny C, Kenel C, Leinenbach C, Jhabvala J, Logé RE (2017) 3D Laser Shock Peening – A new method for the 3D control of residual stresses in Selective Laser Melting. Mater Des 130:350–356
4. Stoudt MR, Lass EA, Ng DS, Williams ME, Zhang F, Campbell CE, Lindwall G, Levine LE (2018) The influence of annealing temperature and time on the formation of δ-phase in additively-manufactured inconel 625. Metall and Mater Trans A 49(7):3028–3037
5. James M, Lu J, Roy G (1996) Handbook of Measurement of Residual stresses. In: Lu J (ed) Lilburn, Georgia: The Fairmount Press
6. Withers PJ, Bhadeshia HKDH (2001) Residual stress: Part 1 – Measurement techniques. Mater Sci Technol 17:355–365
7. Rossini NS, Dassisti M, Benyounis KY, Olabi AG (2012) Methods of measuring residual stresses in components. Mater Des 35:572–588
8. Prime MB (2001) Cross-sectional mapping of residual stresses by measuring the surface contour after a cut. J Eng Mater Technol 123(2):162–168
9. Toparli MB, Fitzpatrick ME, Gungor S (2013) Improvement of the contour method for measurement of near-surface residual stresses from laser peening. Exp Mech 53(9):1705–1718
10. Geng P, Morimura M, Ma N, Huang W, Li W, Narasaki K, Ogura T, Aoki Y, Fujii H (2022) Measurement and simulation of thermal-induced residual stresses within friction stir lapped Al/steel plate. J Mater Process Technol 310:117760
11. Kartal ME, Turski M, Johnson G, Fitzpatrick ME, Gungor S, Withers PJ, Edwards L (2006) Residual stress measurements in single and multi-pass groove weld specimens using neutron diffraction and the contour method. Mater Sci Forum 524–525:671–676
12. Woo W, Choo H, Prime MB, Feng Z, Clausen B (2008) Microstructure, texture and residual stress in a friction-stir-processed AZ31B magnesium alloy. Acta Mater 56(8):1701–1711
13. Smith WL, Roehling JD, Strantza M, Ganeriwala RK, Ashby AS, Vrancken B, Clausen B, Guss GM, Brown DW, McKeown JT, Hill MR, Matthews MJ (2021) Residual stress analysis of in situ surface layer heating effects on laser powder bed fusion of 316L stainless steel. Addit Manuf 47:102252
14. Teixeira J, Maréchal D, Wimpory RC, Denis S, Lefebvre F, Frappier R (2022) Formation of residual stresses during quenching of Ti17 and Ti–6Al–4V alloys: Influence of phase transformations. Mater Sci Eng 832:142456
15. Zabeen S, Preuss M, Withers PJ (2013) Residual stresses caused by head-on and 45° foreign object damage for a laser shock peened Ti–6Al–4V alloy aerofoil. Mater Sci Eng, A 560:518–527
16. Traore Y, Paddea S, Bouchard PJ, Gharghouri MA (2013) Measurement of the residual stress tensor in a compact tension weld specimen. Exp Mech 53(4):605–618
17. Chighizola CR, Hill MR (2022) Two-dimensional mapping of bulk residual stress using cut mouth opening displacement. Exp Mech 62:75–86
18. Vasileiou AN, Smith MC, Francis JA, Balakrishnan J, Wang YL, Obasi G, Burke MG, Pickering EJ, Gandy DW, Irvine NM (2021) Development of microstructure and residual stress in electron beam welds in low alloy pressure vessel steels. Mater Des 209:109924
19. Javadi Y, Smith MC, Abburi Venkata K, Naveed N, Forsey AN, Francis JA, Ainsworth RA, Truman CE, Smith DJ, Hosseinzadeh F, Gungor S, Bouchard PJ, Dey HC, Bhaduri AK, Mahadevan S (2017) Residual stress measurement round robin on an electron beam welded joint between austenitic stainless steel 316L(N) and ferritic steel P91. Int J Press Vessels Pip 154:41–57

20. Kartal ME (2013) Analytical solutions for determining residual stresses in two-dimensional domains using the contour method. Proc Roy Soc A: Math Phys Eng Sci 469:2159
21. Nadammal N, Cabeza S, Mishurova T, Thiede T, Kromm A, Seyfert C, Farahbod L, Haberland C, Schneider JA, Portella PD, Bruno G (2017) Effect of hatch length on the development of microstructure, texture and residual stresses in selective laser melted superalloy Inconel 718. Mater Des 134:139–150
22. Lu Y, Wu S, Gan Y, Huang T, Yang C, Junjie L, Lin J (2015) Study on the microstructure, mechanical property and residual stress of SLM Inconel-718 alloy manufactured by differing island scanning strategy. Opt Laser Technol 75:197–206
23. Goel S, Neikter M, Capek J, Polatidis E, Colliander MH, Joshi S, Pederson R (2020) Residual stress determination by neutron diffraction in powder bed fusion-built Alloy 718: influence of process parameters and post-treatment. Mater Des 195:109045
24. Georgilas K, Khan RHU, Kartal ME (2020) The influence of pulsed laser powder bed fusion process parameters on Inconel 718 material properties. Mater Sci Eng A 769:138527
25. Georgilas G, Sergi A, Khan RHU, Kartal ME (2022) Investigation of novel post-thermal treatments of alloy 718 fabricated by modulated laser powder bed fusion. Mater Sci Eng A 849:143502
26. A International (2013)ASTM E837 - 13a Standard Test Method for Determining Residual Stresses by the Hole-Drilling Strain-Gage Method. ASTM International, West Conshohocken, PA
27. Kartal ME, Kang Y-H, Korsunsky AM, Cocks ACF, Bouchard JP (2016) The influence of welding procedure and plate geometry on residual stresses in thick components. Int J Solids Struct 80:420–429
28. Uzun F, Everaerts J, Brandt LR, Kartal ME, Salvati E, Korsunsky AM (2018) The inclusion of short-transverse displacements in the eigenstrain reconstruction of residual stress and distortion in in740h weldments. J Manuf Process 36:601–612
29. Kartal ME (2008) Advanced experimental methods for the characterization of welded structures. The Open University, PhD Thesis, Milton Keynes
30. Hosseinzadeh F, Kowal J, Bouchard PJ (2014) Towards good practice guidelines for the contour method of residual stress measurement. J Eng 2014(8):453–468
31. Kartal ME, Liljedahl CMD, Gungor S, Edwards L, Fitzpatrick ME (2008) Determination of the profile of the complete residual stress tensor in a VPPA weld using the multi-axial contour method. Acta Mater 56(16):4417–4428
32. Hall CA, Meyer WW (1976) Optimal error bounds for cubic spline interpolation. J Approx Theory 16(2):105–122
33. de Boor C (2004) Spline Toolbox User's Guide, 3.2.1. The Mathworks Inc, Natick, MA
34. Prime MB, DeWald AT (2013) The Contour Method. In: Schajer GS (ed) Practical Residual Stress Measurement Methods. John Wiley & Sons, Ltd., Chennai, India, pp 109–138
35. Collins PC, Brice DA, Samimi P, Ghamarian I, Fraser HL (2016) Microstructural control of additively manufactured metallic materials. Annu Rev Mater Res 46(1):63–91
36. Gu D (2015) Laser additive manufacturing of high-performance materials. Springer, Berlin, Heidelberg
37. Ding D, Pan Z, Cuiuri D, Li H (2015) Wire-feed additive manufacturing of metal components: technologies, developments and future interests. Int J Adv Manuf Technol 81(1–4):465–481
38. Salmi A, Atzeni E, Iuliano L, Galati M (2017) Experimental Analysis of Residual Stresses on AlSi10Mg Parts Produced by Means of Selective Laser Melting (SLM). Procedia CIRP 62:458–463
39. Robinson J, Ashton I, Fox P, Jones E, Sutcliffe C (2018) Determination of the effect of scan strategy on residual stress in laser powder bed fusion additive manufacturing. Addit Manuf 23:13–24
40. Karabulut Y, Kaynak Y (2020) Drilling process and resuling surface properties of Inconel 718 alloy fabricated by Selective Laser Melting Additive Manufacturing. Procedia CIRP 87:355–359
41. Yavelak JJ (1985) Bulk-Zero Stress Standard—AISI 1018 Carbon-Steel Specimens, Round Robin Phase 1. Exp Tech 9(4):38–41
42. Flaman MT, Herring JA (1986) SEM/ASTM Round-Robin Residual-Stress-Measurement Study—Phase 1, 304 Stainless-Steel Specimen. Exp Tech 10(5):23–25
43. Fang ZC, Wu ZL, Huang CG, Wu CW (2020) Review on residual stress in selective laser melting additive manufacturing of alloy parts. Opt Laser Technol 129:6283
44. Hosseinzadeh F, Ledgard P, Bouchard PJ (2013) Controlling the cut in contour residual stress measurements of electron beam welded Ti-6Al-4V alloy plates. Exp Mech 53:829–839

Publisher's Note Springer Nature remains neutral with regard to jurisdictional claims in published maps and institutional affiliations.